Supplementary Information

S1. EXPERIMENTAL SETUP

To conduct the experiments we use the experimental setup shown in Fig. S1. We perform both time resolved and time integrated experiments. In the following we describe only the time integrated measurements reported in Fig. S4. The time resolved measurements [Figs. 1(a-l)] have been described in the main manuscript (see Section II, "Sample and Experiment" for details).

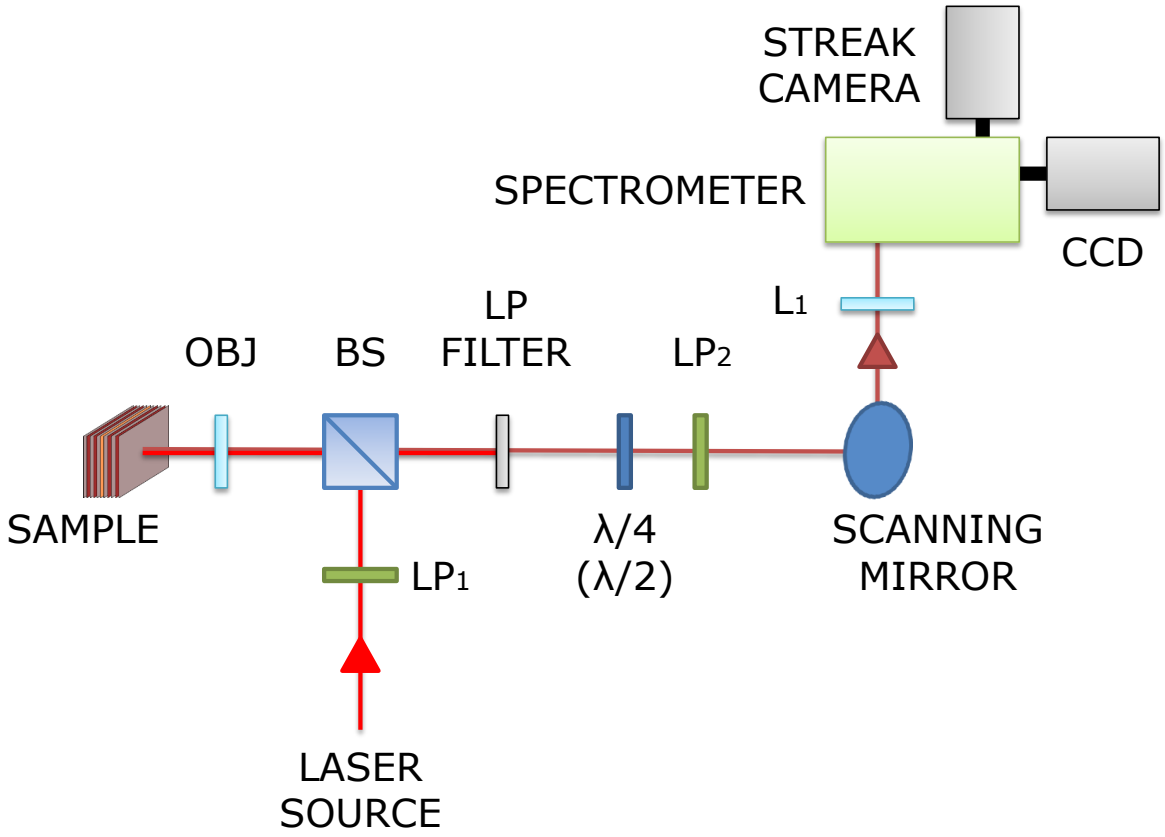

Figure **S1**. Sketch of the setup used in the experiments. Lists of the optical components: **OBJ** is the 20x, 0.4 NA objective; **BS** is the non-polarizing beam splitter; **LP FILTER** is the long pass filter to filter the excitation laser out; $\lambda/4$ ($\lambda/2$) is the quarter-wave (half-wave) plate; $\mathbf{LP}_{1,2}$ are the linear polarizers and **L1** is the 10 cm focal length lens.

In the time integrated experiments (Figs. S4), the excitation is provided by a single-mode narrow-linewidth CW laser, chopped with a duty cycle of 0.1 to reduce sample heating. The horizontal linearly polarized excitation, with polarization parallel to the x-axis (see Figs. S4), is tuned to the first reflectivity minimum above the stopband of the DBR, at 1.687 eV (i.e., non resonant excitation), and focused to a ~ 2 μm FWHM spot by a 0.4 numerical aperture objective. The sample is held in a cold-finger cryostat at a temperature of $T \approx 6$ K. The polarized emission is collected in reflection geometry through the same objective and analyzed by a polarimeter composed of a $\lambda/2$ or $\lambda/4$ plate and a Wollaston prism, with $\sim 20°$ polarization splitting angle. The emission is then imaged in real space by a 10 cm focus lens directly on a CCD camera (time integrated measurements). In this way, both the polarization components are imaged simultaneously and the Stokes parameters calculated in real time by an appropriate software.

S2. TOTAL HALF-SKYRMION TEXTURES

In Fig. 2 of the main manuscript we have shown the vector field of the total pseudospin vector **S** calculated over the first quadrant. In Fig. **S2**(a) we report the vector field of the total pseudospin vector **S** in all the quadrants of the x-y plane, together with the circular stokes component S_z in Fig. **S2**(b), showing the half-skyrmion topological indices calculated by means of the integral (Eq.5) of the article. The vector field of the total pseudospin vector reveals the presence of an ordered pattern composed of half-skyrmions, with topological index $N_{sk} = \pm 0.5$.

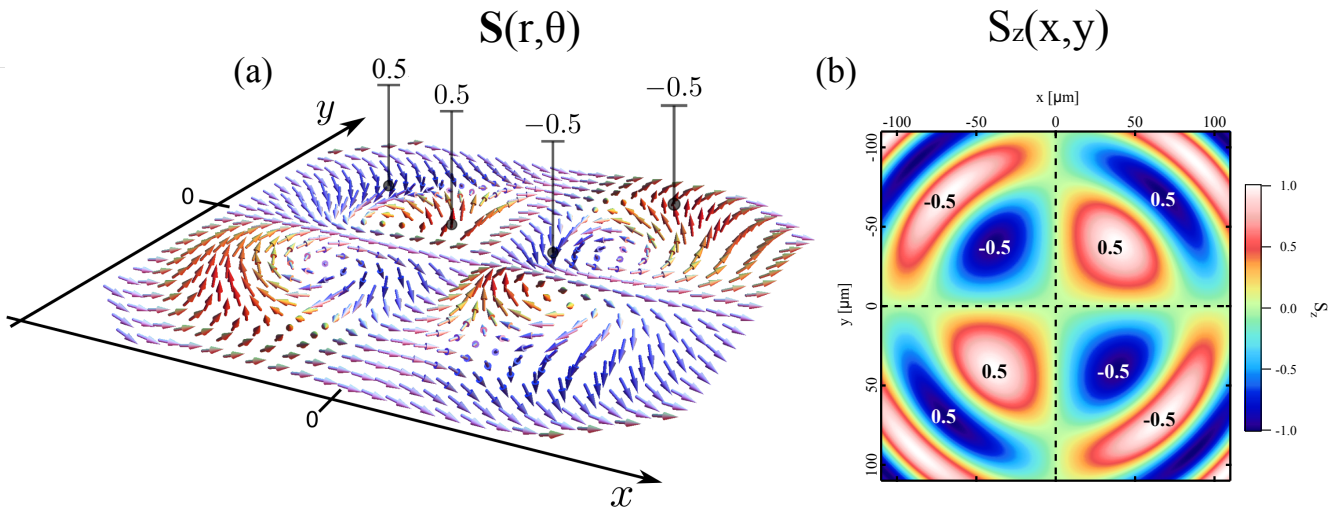

Figure **S2**. (a) The vector field of the two-dimensional polariton half-skyrmions, showing the rotation of the total pseudospin vector $\mathbf{S}(r,\theta) = (S_x, S_y, S_z)$ in the x-y microcavity plane. The different colors of the vectors refer to the different polarization domains. In particular, red and blue refer to the circular polarizations S_z (with opposite orientations along the z axis), while the other colors to the linear polarization components S_x (lying in the x-y plane), and the diagonal polarization S_y (oriented at $\pm 45^\circ$ respect to the x-y plane). (b) Circular Stokes component S_z showing the half-skyrmion topological indices calculated for each spin lobe by means of the integral (Eq.5) in the main manuscript.

The sign of the topological number N_{sk} is determined by the S_z rotation from the half-skyrmion core towards the spin-lobe boundary, and the rotation of the in-plane pseudospin (S_x, S_y) along a closed path inside the lobe containing the half-skyrmion core. For example, the first lobe in the positive x-y quadrant (colored blue) shows S_z rotating from -1 to zero at the boundary of neighboring spin lobes. Around the half-skyrmion core, the in-plane pseudospin completes one counterclockwise rotation. Together, these give $N_{sk} = (-0.5) \times (1)$. In the next lobe (red), these have switched rotations and one gets $N_{sk} = (0.5) \times (-1)$.

An approximate analytical expression of $\mathbf{S}(r,\theta)$ for our non-resonant excitation can be associated with the solution of polaritons populating a single energy on a ring in k-space (see Ref. [1]) where the polariton pseudospin field of the optical spin Hall effect can be described by:

$$\mathbf{S}(r,\theta) = \left[\cos^2(2\theta) + \sin^2(2\theta)\cos(\xi r)\right]\hat{\mathbf{x}} + \left[\sin(4\theta)\sin^2(\xi r/2)\right]\hat{\mathbf{y}} - \left[\sin(2\theta)\sin(\xi r)\right]\hat{\mathbf{z}} \tag{1}$$

with r and θ being the system polar coordinates and ξ an arbitrary constant corresponding to the period of the S_z

spin rotating along the x-y system diagonal. Plugging $\mathbf{S}(r,\theta)$ into Eq.5 of the main manuscript results in:

$$\begin{aligned} N_{sk} = \frac{\xi}{4\pi}\int \Big[& -2\cos^4(2\theta)\sin(2\theta)\sin^2(\xi r) \\ & + 4\cos^4(2\theta)\sin(2\theta)\cos(\xi r)\sin^2\left(\frac{\xi r}{2}\right) \\ & - 4\cos^2(2\theta)\sin^3(2\theta)\cos(\xi r)\sin^2\left(\frac{\xi r}{2}\right) \\ & - 2\cos^2(2\theta)\sin^3(2\theta)\cos(\xi r)\sin^2(\xi r) \\ & + 4\cos^2(2\theta)\sin^3(2\theta)\cos^2(\xi r)\sin^2\left(\frac{\xi r}{2}\right) \\ & - 4\sin^5(2\theta)\cos^2(\xi r)\sin^2\left(\frac{\xi r}{2}\right) \\ & - 4\cos^2(2\theta)\sin^3(2\theta)\sin^2(\xi r)\sin^2\left(\frac{\xi r}{2}\right) \\ & + 16\cos^2(2\theta)\sin^3(2\theta)\cos(\xi r)\sin^4\left(\frac{\xi r}{2}\right) \\ & - 4\sin^3(2\theta)\sin^2(\xi r)\sin^2\left(\frac{\xi r}{2}\right)\Big] dr d\theta \end{aligned} \tag{2}$$

Integration across individual spin lobes, $\theta \in [n \rightarrow\ (n+1)]\pi/2$ and $r \in [m \rightarrow (m+1)]\pi/\xi$ with $n, m \in \mathbb{N}$, gives:

$$N_{sk} = \frac{(-1)^n}{60}\Big[-3-3+2+0+2-8-2-8-10\Big] = \frac{(-1)^{n+1}}{2}, \tag{3}$$

which shows the half-integer nature of the spin-lobes, confirming the presence of half-skyrmions. One can see that the sign of N_{sk} only depends on which quadrant the spin lobe resides.

S3. OPTICAL SPIN HALL EFFECT

One of the main effects affecting the spin dynamics of polaritons is the so called *optical spin Hall effect* (OSHE). The OSHE, predicted by Kavokin and co-workers in 2005[2] and experimentally observed in both polaritonic [3] and photonic [4] microcavities, consists in the precession of the polariton pseudospin in the plane of the microcavity. The effect is enabled by the energy splitting between transverse-electric (TE) and transverse-magnetic (TM) polarized modes [5] and the longitudinal-transverse splitting of the exciton states inside the microcavity[6]. The TE-TM splitting arises from the fact that different polarized optical modes will have different phase and penetrations into the Bragg mirrors. The splitting of the excitonic states, on the other hand, is mainly due to the long-range exciton exchange interaction and arises from the different alignment of the dipole moments (i.e., exciton states having dipole moments in different directions will have different energies[7]).
In the case of polariton microcavities, the TE-TM splitting (Δ_{LT}) acts as a wave vector dependent effective magnetic field ($\mathbf{H_{eff}}$), making the pseudospin of polaritons precess if the latter is not parallel to it[2]. To take into account the precession of the pseudospin induced by the OSHE, polaritons propagation in microcavities is described by the following effective Hamiltonian[2]:

$$\widehat{H} = \frac{\hbar^2 k^2}{2m^*} + \mu_B\, g(\boldsymbol{\sigma}\cdot\mathbf{H_{eff}}), \tag{4}$$

where m^* is the polariton effective mass, μ_B the Bohr magneton, g the effective exciton Zeeman factor, $\boldsymbol{\sigma}$ the Pauli matrix vector and $\mathbf{H_{eff}}$ the effective magnetic field[2]:

$$\mathbf{H_{eff}} = \frac{\hbar}{\mu_B\, g}\mathbf{\Omega_k} \tag{5}$$

and $\mathbf{\Omega_k}$, which lies in the plane of the microcavity and has the following components[2]:

$$\Omega_x = \frac{\Delta_{LT}}{\hbar k^2}(k_x^2 - k_y^2), \qquad \Omega_y = \frac{\Delta_{LT}}{\hbar k^2}\, 2k_x k_y, \qquad \Omega_z = 0. \tag{6}$$

Here, $\vec{k} = (k_x, k_y)$ is the in-plane polariton wave vector. As indicated by equation 6, the orientation of the effective magnetic field in the plane of the microcavity, depends on the direction of the polariton wave vector, whose components are:

$$k_x = k\,\cos\theta, \qquad k_y = k\,\sin\theta, \qquad k_z = 0, \tag{7}$$

with θ being the angle between $\vec{k}$ (the direction of propagation) and the k_x-axis [see Figs.**S3**]. Thus, by combining equation 6 and equation 7, the components of the effective magnetic field ($\mathbf{\Omega_k}$) can be determined[8]:

$$\Omega_x = \frac{\Delta_{LT}}{\hbar}\,\cos(2\theta), \qquad \Omega_y = \frac{\Delta_{LT}}{\hbar}\,\sin(2\theta), \qquad \Omega_z = 0 \tag{8}$$

Equation 8 determines the orientation of the effective magnetic field in the plane of the microcavity, which depends on the direction of the polariton wave vector. The values of the effective magnetic field, calculated for different angles of propagation of polaritons, are reported in the table I (for the first and second quarter) and schematically represented in Fig. **S3**(a).

Table I. Distribution of the effective magnetic field in the k_x-k_y plane as function of the angle θ, which defines the direction of propagation of polaritons [see Fig. **S3**(a)].

Angle	Ω_x	Ω_y
$\theta = 0$	$\frac{\Delta_{LT}}{\hbar}$	0
$\theta = \frac{\pi}{4}$	0	$\frac{\Delta_{LT}}{\hbar}$
$\theta = \frac{\pi}{2}$	$-\frac{\Delta_{LT}}{\hbar}$	0
$\theta = \frac{3\pi}{4}$	0	$-\frac{\Delta_{LT}}{\hbar}$
$\theta = \pi$	$\frac{\Delta_{LT}}{\hbar}$	0

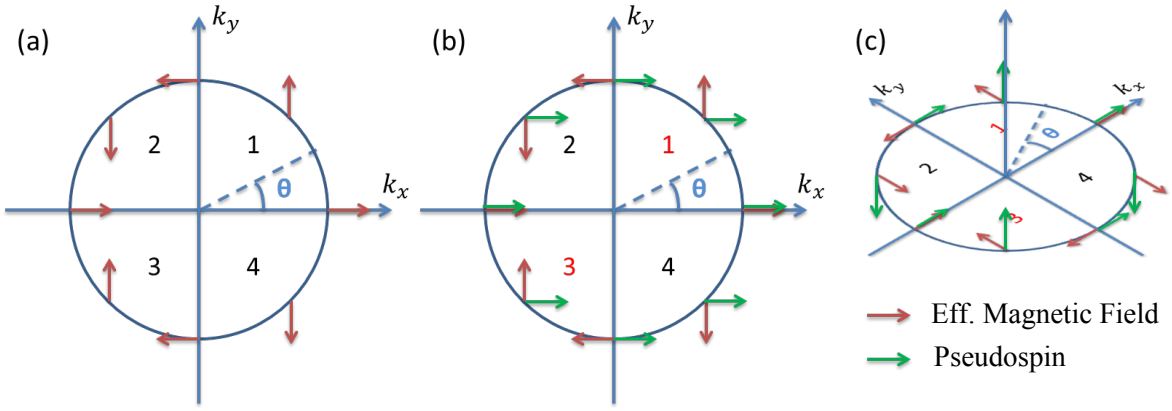

Figure **S3**. (a) The red arrows show the distribution of the effective magnetic field in k-space induced by the TE-TM splitting (see equation 8). (b) The green arrows indicate the linearly polarized pseudospin (i.e., the pseudospin is parallel to the x-axis) while the red arrow correspond to the effective magnetic field. Note that at at $\theta = \pi/4, 3\pi/4, 5\pi/4, 7\pi/4$ (i.e., along the diagonal directions with respect to the coordinates axes) the pseudospin is perpendicular to the effective magnetic field. (c) The initially linearly polarized pseudospin precess and, due to the orientation of the effective magnetic field, it becomes parallel to the z direction in the quarters 1 and 3 and antiparallel to the z axis in the quarters 2 and 4. Thus, the first quarters (1,3) correspond to σ_+ while the other quarters (2,4) to σ_- circularly polarized emission. Images adapted and redrawn from Ref.[2].

The TE-TM splitting of the polariton dispersion is zero at $\vec{k}=0$ and increases as a function of k, following a square root law at large k[7]. Since the magnitude of the effective magnetic field ($\mathbf{\Omega_k}$) is proportional to the TE-TM splitting ($\frac{\Delta_{LT}}{\hbar}$), also $\mathbf{\Omega_k}$ is zero at $k = 0$. By means of a tightly focused excitation spot, a radially expanding polariton condensate can be generated with a well defined wave vector. Since the orientation of the effective magnetic field depends on the polariton wave vectors (equation 6), polaritons propagating in different directions experience different effective magnetic fields, which correspond to rotation of the pseudospin in different directions. In particular, polaritons propagating in opposite directions (i.e., at opposite angles θ) experience precession in opposite directions [first and second quarter in Fig.**S3**(b)]. This results to an angular dependent polarized emission of the polaritons and, consequently, to the appearance of alternating circularly or linearly polarized domains in the plane of the microcavity. Thus, different polarized spin domains develop in different quadrants of the x-y plane [Fig.**S3**(c)].

S4. SPIN TEXTURES UNDER CW EXCITATION

We repeat the same experiment described in the main manuscript, but now exciting with a CW laser at power $5\times P_{Thr}$ (with $P_{Thr} \approx 15$ mW).

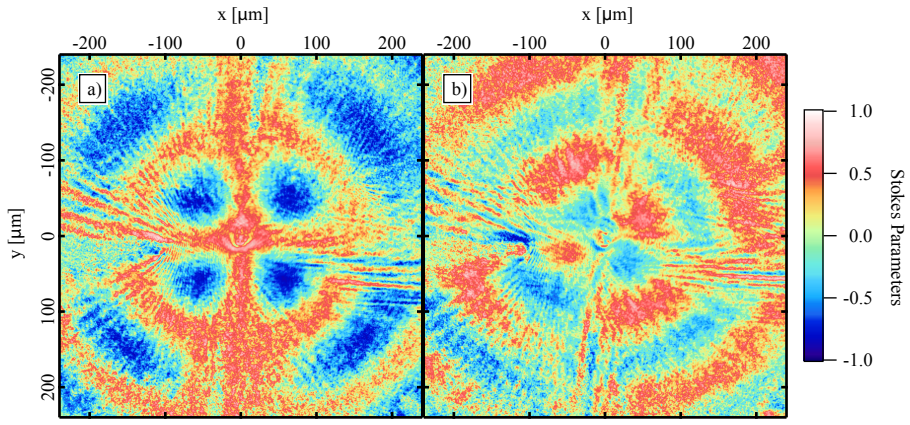

Figure **S4**. Experimental linear (a) and circular (b) Stokes parameters showing the formation of 2D pseudospin textures in real space. The excitation beam is linearly polarized and at 1.687 eV.

In CW experiments, polaritons decayed or emitted from the cavity are continuously replenished by the CW excitation so that, once a macroscopic ground state population is reached, i.e., the relaxation rate of polaritons into the ground state becomes greater than its radiative decay rate, a steady state polariton population is formed. In this case, the generation of polaritons is sustained by the continuously injection of electron-hole pairs due to the nonresonant CW laser, allowing us to observe the polariton spin to precess twice respect to its initial orientation [Figs. **S4**(a) and (b)]. This corresponds to the appearance of additional features (e.g., the external blue lobes in Figs. **S4**(a)) compared to the one observed in Figs.1(a-l) of the main manuscript.

S5. SPIN TEXTURES IN PRESENCE OF DISORDER

In Fig. **S5**(a-c), the formation of the polariton spin textures shown in the main manuscript [Figs.1(m-o)] is calculated in the presence of disorder. The parameters used to perform the simulations are the same used for Figs. 1(m-o) of the main manuscript[9].

The disorder potential was generated with 0.05 meV root mean squared amplitude and 1.5 μm correlation length[10]. The theoretical calculations show that disorder generates additional features in the spin textures, as in the case of

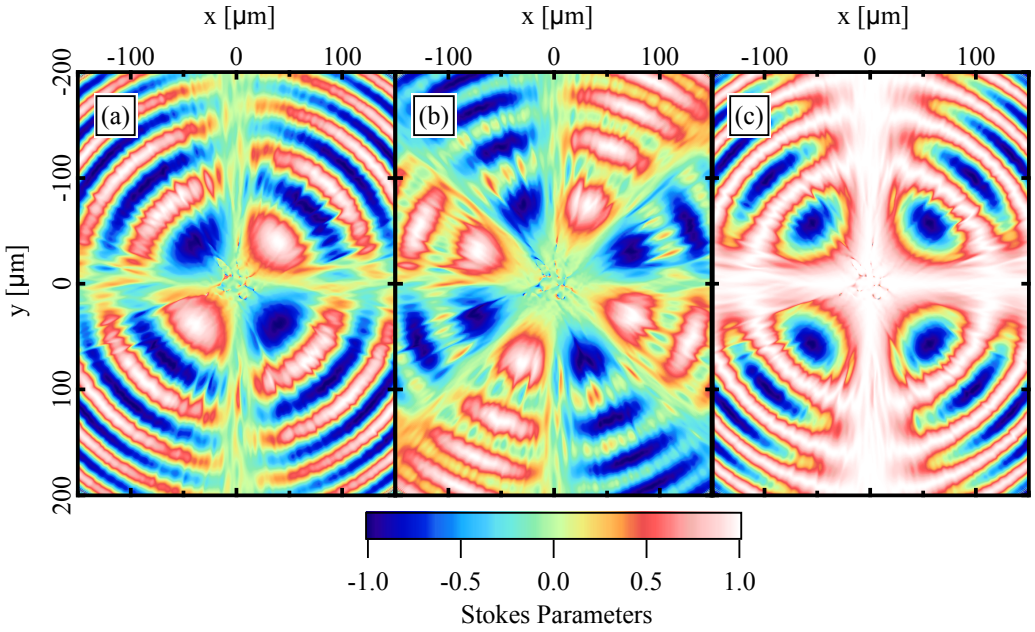

Figure **S5**. Theoretical real space circular (a), diagonal (b) and linear (c) Stokes parameters calculated using Eqs. 2-4 from main manuscript in presence of disorder 34 ps after excitation with $P_+/P_- = 1$ and $P_+,\ P_- > 0$.

the experimental data reported in Figs.**S4**.

---

[1] H. Flayac, D. D. Solnyshkov, I. A. Shelykh, and G. Malpuech, Phys. Rev. Lett. **110**, 016404 (2013).
[2] A. Kavokin, G. Malpuech, and M. Glazov, Phys. Rev. Lett. **95**, 136601 (2005).
[3] C. Leyder, M. Romanelli, J. P. Karr, E. Giacobino, T. C. H. Liew, M. M. Glazov, A. V. Kavokin, G. Malpuech, and A. Bramati, Nature Physics **3**, 628 (2007).
[4] M. Maragkou, C. E. Richards, T. Ostatnický, A. J. D. Grundy, J. Zajac, M. Hugues, W. Langbein, and P. G. Lagoudakis, Opt. Lett. **36**, 1095 (2011).
[5] G. Panzarini, L. C. Andreani, A. Armitage, D. Baxter, M. S. Skolnick, V. N. Astratov, J. S. Roberts, A. V. Kavokin, M. R. Vladimirova, and M. A. Kaliteevski, Phys. Rev. B **59**, 5082 (1999).
[6] M. Z. Maialle, E. A. de Andrada e Silva, and L. J. Sham, Phys. Rev. B **47**, 15776 (1993).
[7] K. V. Kavokin, I. A. Shelykh, A. V. Kavokin, G. Malpuech, and P. Bigenwald, Phys. Rev. Lett. **92**, 017401 (2004).
[8] In the calculations the following trigonometric relations have been used: $cos^2(\theta) - sin^2(\theta) = cos(2\theta)$ and $2\,cos(\theta)\,sin(\theta) = sin(2\theta)$.
[9] *In all the theoretical calculations the following parameters were set to:* $\alpha = 2.4\ \mu eV\ \mu m^2$, $g_R = 1.5\alpha$, $G = 4\alpha$, $r_c = 0.01\ \mu m^2\ ps^{-1}$, $\Delta_{LT}/k_{LT}^2 = 11.9\ \mu eV\ \mu m^2$, $\tau_p = 3.8\ ps$, $\tau_x = 10\ ps$.
[10] V. Savona and W. Langbein, Phys. Rev. B **74**, 075311 (2006).